DOI 10.1007/s10946-024-10184-8
Journal of Russian Laser Research, Volume 45, Number 1, January, 2024

POPULATION DISTRIBUTION AND SPLITTING NONLINEARITY FOR RYDBERG ATOMIC GAS UNDER MULTIPLE FIELDS

Chao Li,* Guo Ma, Yunyun Zhang, and Shengzhao Wang

School of Mathematics and Science, Nanyang Institute of Technology Nanyang 473000, China

*Corresponding author e-mail: lichao@nyist.edu.cn

Abstract

Rydberg atom has a very large polarizability proportional to n^7 (n is the principal quantum number), the energy interval between adjacent energy levels is in the microwave frequency band, and the transition between adjacent energy levels has a huge dipole moment proportional to n^4; as a result, the Rydberg atom is extremely sensitive to the external field, making it an important means of microwave detection. The interaction of Rydberg atoms with laser fields can be described within the framework of density matrix theory. In this paper, based on a four-level system with multiple laser fields, we study the relationship between the population distribution of different energy levels and the detuning of the coupling field, as well as the effect of the Rabi frequency of microwave field on the electromagnetically induced transparency (EIT) signal by solving the density matrix of the steady state system. Considering the characteristics of density matrix, we assume that the diagonal elements are real and the off-diagonal elements are complex. We find that the operation efficiency of this construction method is twice as high as that of the direct representation by complex numbers. At the same time, we obtain that the Rabi frequency of microwave electric field is proportional to the splitting of EIT signal within a certain range.

Keywords: Rydberg atom, electromagnetically induced transparency, density matrix, linear equations.

1. Introduction

Rydberg atom is an atom in a highly excited state (principal quantum number n is large) with a very high electron transition orbit, and therefore it has long energy level lifetime ($\sim n^3$) [1], large radius size ($\sim n^2$), large polarization ($\sim n^7$), large transition dipole moment ($\sim n^4$), and other characteristics [1]. In addition, Rydberg atoms have strong interactions with each other, which lead to excitation blocking effect. These characteristics make Rydberg atom a research hot spot playing an extremely important role in semiconductor physics, surface physics, spectroscopy, quantum information, quantum computing [2, 3], and many other research fields. Also, due to the singularity of Rydberg atom itself, the electromagnetically-induced transparency effect produced by Rydberg atom gas has an important characteristic, which is different from ordinary EIT. Therefore, Rydberg atoms have a very wide application prospect in the fields of quantum entanglement, quantum logic gates [4], single-photon source preparation, and quantum precision measurement [5]. Based on the large polarizability [1, 6–8] of the Rydberg atom, it is extremely sensitive to external fields and is easily regulated by the external field. In addition, the Rydberg atomic level interval is very small, and the transition frequency between Rydberg levels can be

Manuscript submitted by the authors in English on November 19, 2023.

covered by microwave signals, so the microwave electric field can be measured through the microwave electric field coupling Rydberg state.

The EIT phenomenon is a typical quantum coherent effect [9], the essence of which is that the strong coupling laser affects the dispersion property of the absorbing medium, so that the absorption of the weak probe laser is reduced or even completely transparent. The EIT effect was first proposed in 1989 [10], and the EIT phenomenon had been experimentally implemented, using Strontium (Sr) atoms in 1991 [11]. The Rydberg atoms are very sensitive to the external field, so they are important in the field detection. In 2012, T. Puffer, J. P. Shaffer, et al. experimentally proved a new microwave measurement method based on Rydberg atomic EIT for the first time [12]. The microwave field is coupled with the corresponding two Rydberg states, so that the Autler–Townes (AT) splitting occurs in the EIT spectrum. By measuring the splitting of the EIT spectrum, the size of the microwave field can be deduced in reverse. The sensitivity of microwave field measurement is about 30 $\mu V \cdot cm^{-1} \cdot Hz^{-1/2}$, the minimum measured microwave field is 8 $\mu V \cdot cm^{-1}$ [12]. In 2016, the group of G. Raithel and NIST jointly reported the strong microwave field measurement based on Rydberg atom EIT, whose maximum measurable intensity reached 230 V/m, about 20% higher than the microwave ionization limit of Rubidium atom [13]. The EIT phenomenon with Rydberg atoms, using Rubidium (Rb) atomic vapor pool, was first observed in experiment in 2006, which achieved all-optical nondestructive measurement [14]. Subsequently, the EIT effect of Rydberg atom was further studied in atomic beam [15] and cold atom [16] systems.

In this paper, we study the influence of laser field intensity on the population distribution and the double peak splitting of EIT signal by numerical simulation based on the density matrix theory of light–matter interaction in a stepped multilevel system under the action of two-photon laser fields. In the process of numerical calculation, we adopt a new method of matrix construction. By artificial assuming the diagonal elements to be real, the calculation results are much closer to physics reality.

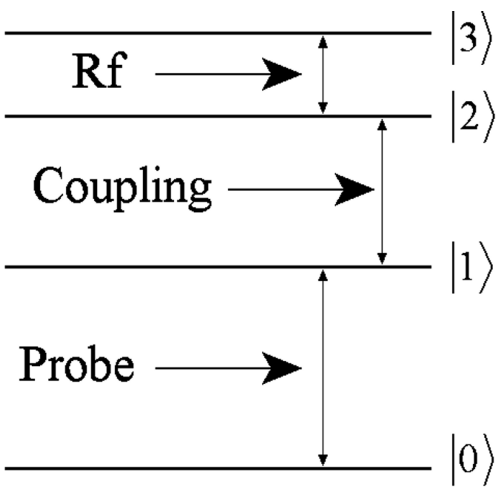

Fig. 1. Energy level diagram of a ladder four-level system.

2. Theoretical Model

In Fig. 1, we show the most welcome scheme of the system levels used in the measurement of microwave electric field. Here, "Probe" means the tunable detection laser to excite Rydberg atoms from the ground state $|0\rangle$ to the intermediate state $|1\rangle$. Coupling refers to the coupling laser, which excites Rydberg atoms from intermediate state $|1\rangle$ to the Rydberg state $|2\rangle$, Rf is the microwave field to be measured, which can excite atoms from Rydberg state $|2\rangle$ to Rydberg state $|3\rangle$. Then, the evolution equation of the density matrix for this system reads

$$\dot{\rho} = \frac{\partial \rho}{\partial t} = -\frac{i}{\hbar}[H, \rho] + \zeta, \tag{1}$$

where H represents the Hamiltonian of the Rydberg atomic system, and ζ is the Lindblad operator describing the decay process. The system Hamiltonian and density matrix are [17,18]

$$H = \frac{\hbar}{2}\begin{pmatrix} 0 & \Omega_p & 0 & 0 \\ \Omega_p & -2\Delta_p & \Omega_c & 0 \\ 0 & \Omega_c & -2(\Delta_p+\Delta_c) & \Omega_{Rf} \\ 0 & 0 & \Omega_{\mathrm{Rf}} & -2(\Delta_p+\Delta_c+\Delta_{\mathrm{Rf}}) \end{pmatrix}, \qquad \rho = \begin{pmatrix} \rho_{11} & \rho_{12} & \rho_{13} & \rho_{14} \\ \rho_{21} & \rho_{22} & \rho_{23} & \rho_{24} \\ \rho_{31} & \rho_{32} & \rho_{33} & \rho_{34} \\ \rho_{41} & \rho_{42} & \rho_{43} & \rho_{44} \end{pmatrix}, \quad (2)$$

where Ω_p, Ω_c, and Ω_{Rf} represent the Rabi frequency of the probe laser, coupling laser, and microwave source, respectively, and are defined as $\Omega_i = \dfrac{\mathcal{P}}{\hbar|E_i|}$, where $\mathcal{P}$ is the dipole moment of energy level transition, and E_i is the amplitude of the laser field. From this equation, one can see that, theoretically, the intensity of microwave electric field to be measured is proportional to the Rabi frequency Ω_{Rf}. Also, Δ_p, Δ_c, and Δ_{Rf} represent the detuning of the probe laser, coupling laser, and microwave field, which are defined as follows:

$$\Delta_i = \omega_i - \omega_{oi}, \qquad i = p, c, \mathrm{Rf}. \quad (3)$$

Here, ω_i represents the circular frequency of the probe laser, coupling laser, and Rf source, respectively. The ω_{oi} represents the circular frequency corresponding to the transition for $|0\rangle \to |1\rangle$, $|1\rangle \to |2\rangle$, and $|2\rangle \to |3\rangle$.

The Lindblad operator of the system can be expressed as

$$\zeta = \begin{pmatrix} \Gamma_2\rho_{22} & -\gamma_{12}\rho_{12} & -\gamma_{13}\rho_{13} & -\gamma_{14}\rho_{14} \\ -\gamma_{21}\rho_{21} & \Gamma_3\rho_{33}-\Gamma_2\rho_{22} & -\gamma_{23}\rho_{23} & -\gamma_{24}\rho_{24} \\ -\gamma_{31}\rho_{31} & -\gamma_{32}\rho_{32} & \Gamma_4\rho_{44}-\Gamma_3\rho_{33} & -\gamma_{34}\rho_{34} \\ -\gamma_{41}\rho_{41} & -\gamma_{42}\rho_{42} & -\gamma_{43}\rho_{43} & -\Gamma_4\rho_{44} \end{pmatrix}, \quad (4)$$

with the factor γ_{ij}, where Γ_i represents the decay rates of different energy levels of the Rydberg atomic system.

The expression of Lindblad operator and Hamiltonian are substituted into the master equation of density matrix. In a closed system, the number of atoms should be conserved, that is, it satisfies the normalization relation:

$$\rho_{11} + \rho_{22} + \rho_{33} + \rho_{44} = 1. \quad (5)$$

The following 10 equations can be obtained from the master equation:

1. Four diagonal elements

$$\dot{\rho}_{11} = i\frac{\Omega_p}{2}(\rho_{12}-\rho_{21}) + \Gamma_2\rho_{22}, \quad (6)$$

$$\dot{\rho}_{22} = -i\frac{\Omega_p}{2}(\rho_{12}-\rho_{21}) + i\frac{\Omega_c}{2}(\rho_{23}-\rho_{32}) - \Gamma_2\rho_{22} + \Gamma_3\rho_{33}. \quad (7)$$

$$\dot{\rho}_{33} = -i\frac{\Omega_c}{2}(\rho_{23}-\rho_{32}) + i\frac{\Omega_{Rf}}{2}(\rho_{34}-\rho_{43}) - \Gamma_3\rho_{33} + \Gamma_4\rho_{44}, \quad (8)$$

$$\dot{\rho}_{44} = -i\frac{\Omega_{Rf}}{2}(\rho_{34}-\rho_{43}) - \Gamma_4\rho_{44}. \quad (9)$$

Notice that these four equations satisfy $\dot{\rho}_{11} + \dot{\rho}_{22} + \dot{\rho}_{33} + \dot{\rho}_{44} = 0$, so only three of them are independent.

2. Since the density matrix satisfies $\dot{\rho}_{ij} = \dot{\rho}^*_{ji}$, only six off-diagonal elements are as follows:

$$\dot{\rho}_{21} = (i\Delta_p - \gamma_{12})\rho_{12} + i\frac{\Omega_p}{2}(\rho_{22} - \rho_{11}) - i\frac{\Omega_c}{2}\rho_{31}, \tag{10}$$

$$\dot{\rho}_{31} = [i(\Delta_p + \Delta_c) - \gamma_{31}]\rho_{31} + i\frac{\Omega_p}{2}\rho_{32} - i\frac{\Omega_c}{2}\rho_{21} - i\frac{\Omega_{\mathrm{Rf}}}{2}\rho_{41}, \tag{11}$$

$$\dot{\rho}_{41} = [i(\Delta_p + \Delta_c + \Delta_{\mathrm{Rf}}) - \gamma_{41}]\rho_{41} + i\frac{\Omega_p}{2}\rho_{42} - i\frac{\Omega_{\mathrm{Rf}}}{2}\rho_{31}, \tag{12}$$

$$\dot{\rho}_{32} = (i\Delta_c - \gamma_{32})\rho_{32} + i\frac{\Omega_c}{2}(\rho_{33} - \rho_{22}) + i\frac{\Omega_p}{2}\rho_{31} - i\frac{\Omega_{\mathrm{Rf}}}{2}\rho_{42}, \tag{13}$$

$$\dot{\rho}_{42} = [i(\Delta_c + \Delta_{\mathrm{Rf}}) - \gamma_{42}]\rho_{42} + i\frac{\Omega_p}{2}\rho_{41} + i\frac{\Omega_c}{2}\rho_{43} - i\frac{\Omega_{\mathrm{Rf}}}{2}\rho_{32}, \tag{14}$$

$$\dot{\rho}_{43} = (i\Delta_{\mathrm{Rf}} - \gamma_{43})\rho_{43} + i\frac{\Omega_c}{2}\rho_{42} + i\frac{\Omega_{\mathrm{Rf}}}{2}(\rho_{44} - \rho_{33}). \tag{15}$$

3. Method to Solve the Evolution Equation of the Density Matrix

The evolution equation of the density matrix is very complicated, and it is difficult to get an analytical solution. When the system reaches the equilibrium state after a long relaxation time, which means $\dot{\rho}_{ij} = 0$, the numerical method can be used to solve the problem. The density matrix described as function (2) is a complex matrix, but the diagonal elements are real numbers, the off-diagonal elements are complex numbers, instead. Therefore, the density matrix can be written in the following form:

$$\rho = \begin{pmatrix} x_0 & x_4 + ix_5 & x_6 + ix_7 & x_8 + ix_9 \\ x_4 - ix_5 & x_1 & x_{10} + ix_{11} & x_{12} + ix_{13} \\ x_6 - ix_7 & x_{10} - ix_{11} & x_2 & x_{14} + ix_{15} \\ x_8 - ix_9 & x_{12} - ix_{13} & x_{14} - ix_{15} & x_3 \end{pmatrix}. \tag{16}$$

By substituting the density matrix elements defined above into Eqs. (5)–(15), we arrive at the following 10 independent equations:

$$x_0 + x_1 + x_2 + x_3 = 1, \tag{17}$$

$$\Gamma_{22}x_1 - \Omega_p x_5 = 0, \tag{18}$$

$$-\Gamma_2 x_1 + \Gamma_3 x_2 - \Omega_p x_5 - \Omega_c x_{11} = 0, \tag{19}$$

$$-\Gamma_3 x_2 + \Gamma_4 x_3 + \Omega_c x_{11} - \Omega_{\mathrm{Rf}} x_{15} = 0, \tag{20}$$

$$\left(\Delta_p x_5 - \gamma_{21} x_4 - \frac{\Omega_c}{2} x_7\right) + i\left(\Delta_p x_4 + \gamma_{21} x_5 + \frac{\Omega_p}{2} x_1 - \frac{\Omega_p}{2} x_6 - \frac{\Omega_c}{2} x_6\right) = 0, \quad (21)$$

$$\left[(\Delta_p + \Delta_c) x_7 - \gamma_{31} x_6 + \frac{\Omega_c}{2} x_{11} - \frac{\Omega_c}{2} x_5 - \frac{\Omega_{\mathrm{Rf}}}{2} x_9\right] + i\left[(\Delta_p + \Delta_c) x_6 + \gamma_{31} x_7 + \frac{\Omega_p}{2} x_{10} - \frac{\Omega_c}{2} x_4 - \frac{\Omega_{\mathrm{Rf}}}{2} x_8\right] = 0, \quad (22)$$

$$\left[(\Delta_p + \Delta_c + \Delta_{\mathrm{Rf}}) x_9 - \gamma_{41} x_8 + \frac{\Omega_p}{2} x_{13} - \frac{\Omega_{\mathrm{Rf}}}{2} x_7\right] + i\left[(\Delta_p + \Delta_c + \Delta_{Rf}) x_8 + \gamma_{41} x_9 + \frac{\Omega_p}{2} x_{12} - \frac{\Omega_{Rf}}{2} x_6\right] = 0, \quad (23)$$

$$\left[\Delta_c x_{11} - \gamma_{32} x_{10} + \frac{\Omega_p}{2} x_7 - \frac{\Omega_{\mathrm{Rf}}}{2} x_{13}\right] + i\left[\Delta_c x_{10} + \gamma_{32} x_{11} + \frac{\Omega_c}{2} x_2 - \frac{\Omega_c}{2} x_1 + \frac{\Omega_p}{2} x_6 - \frac{\Omega_{\mathrm{Rf}}}{2} x_{12}\right] = 0, \quad (24)$$

$$\left[(\Delta_c + \Delta_{\mathrm{Rf}}) x_{13} - \gamma_{42} x_{12} + \frac{\Omega_p}{2} x_9 + \frac{\Omega_c}{2} x_{15} - \frac{\Omega_{\mathrm{Rf}}}{2} x_{11}\right] + i\left[(\Delta_c + \Delta_{\mathrm{Rf}}) x_{12} + \gamma_{42} x_{13} + \frac{\Omega_p}{2} x_8 + \frac{\Omega_c}{2} x_{14} - \frac{\Omega_{\mathrm{Rf}}}{2} x_{10}\right] = 0, \quad (25)$$

$$\left[\Delta_{\mathrm{Rf}} x_{15} - \gamma_{43} x_{14} + \frac{\Omega_c}{2} x_{13}\right] + i\left[\Delta_{\mathrm{Rf}} x_{14} + \gamma_{43} x_{15} + \frac{\Omega_c}{2} x_{12} - \frac{\Omega_{\mathrm{Rf}}}{2} x_2 + -\frac{\Omega_{\mathrm{Rf}}}{2} x_3\right] = 0. \quad (26)$$

Since only Eqs. (6)–(9) are independent of each other, only Eqs. (5)–(7) are used in the substitution; as a result, Eqs. (18)–(20) are obtained. In addition, from Eqs. (10)–(15) we obtain Eqs. (21)–(26), where the real and imaginary parts of the equation are independent. In the end, we arrive at 16 independent linear equations with column vector

$$x = (x_0, x_1, x_2, x_3, x_4, x_5, x_6, x_7, x_8, x_9, x_{10}, x_{11}, x_{12}, x_{13}, x_{14}, x_{15})^T$$

as the variables, which can be described by the matrix equation of the form $Ax = B$.

For $b = (1, 0, 0, 0, 0, 0, 0, 0, 0, 0, 0, 0, 0, 0, 0, 0)$, the formulation of the coefficient matrix A can be obtained from the corresponding coefficients of the 16 equations described above, namely,

$$A = \begin{pmatrix}
1 & 1 & 1 & 1 & 0 & 0 & 0 & 0 & 0 & 0 & 0 & 0 & 0 & 0 & 0 & 0 \\
0 & \Gamma_2 & 0 & 0 & 0 & -\Omega_p & 0 & 0 & 0 & 0 & 0 & 0 & 0 & 0 & 0 & 0 \\
0 & -\Gamma_2 & \Gamma_3 & 0 & 0 & \Omega_p & 0 & 0 & 0 & 0 & 0 & -\Omega_c & 0 & 0 & 0 & 0 \\
0 & 0 & -\Gamma_3 & \Gamma_4 & 0 & 0 & 0 & 0 & 0 & 0 & 0 & \Omega_c & 0 & 0 & 0 & -\Omega_{\mathrm{Rf}} \\
0 & 0 & 0 & 0 & -\gamma_{21} & \Delta_p & 0 & -\frac{\Omega_c}{2} & 0 & 0 & 0 & 0 & 0 & 0 & 0 & 0 \\
-\frac{\Omega_p}{2} & \frac{\Omega_p}{2} & 0 & 0 & \Delta_p & \gamma_{21} & -\frac{\Omega_c}{2} & 0 & 0 & 0 & 0 & 0 & 0 & 0 & 0 & 0 \\
0 & 0 & 0 & 0 & 0 & -\frac{\Omega_c}{2} & -\gamma_{31} & \Delta_p + \Delta_c & 0 & -\frac{\Omega_{\mathrm{Rf}}}{2} & 0 & \frac{\Omega_p}{2} & 0 & 0 & 0 & 0 \\
0 & 0 & 0 & 0 & -\frac{\Omega_c}{2} & 0 & \Delta_p + \Delta_c & \gamma_{31} & -\frac{\Omega_{\mathrm{Rf}}}{2} & 0 & \frac{\Omega_p}{2} & 0 & 0 & 0 & 0 & 0 \\
0 & 0 & 0 & 0 & 0 & 0 & 0 & -\frac{\Omega_{\mathrm{Rf}}}{2} & -\gamma_{41} & \Delta_p + \Delta_c + \Delta_{\mathrm{Rf}} & 0 & 0 & 0 & \frac{\Omega_p}{2} & 0 & 0 \\
0 & 0 & 0 & 0 & 0 & 0 & -\frac{\Omega_{\mathrm{Rf}}}{2} & 0 & \Delta_p + \Delta_c + \Delta_{\mathrm{Rf}} & \gamma_{41} & 0 & 0 & \frac{\Omega_p}{2} & 0 & 0 & 0 \\
0 & 0 & 0 & 0 & 0 & 0 & 0 & \frac{\Omega_p}{2} & 0 & 0 & -\gamma_{32} & \Delta_c & 0 & \frac{\Omega_{\mathrm{Rf}}}{2} & 0 & 0 \\
0 & -\frac{\Omega_c}{2} & \frac{\Omega_c}{2} & 0 & 0 & 0 & \frac{\Omega_p}{2} & 0 & 0 & 0 & \Delta_c & \gamma_{32} & -\frac{\Omega_{\mathrm{Rf}}}{2} & 0 & 0 & 0 \\
0 & 0 & 0 & 0 & 0 & 0 & 0 & 0 & 0 & \frac{\Omega_p}{2} & 0 & -\frac{\Omega_{\mathrm{Rf}}}{2} & -\gamma_{42}\Delta_c + \Delta_{\mathrm{Rf}} & 0 & \frac{\Omega_c}{2} & \\
0 & 0 & 0 & 0 & 0 & 0 & 0 & 0 & \frac{\Omega_p}{2} & 0 & -\frac{\Omega_{\mathrm{Rf}}}{2} & 0 & \Delta_c + \Delta_{\mathrm{Rf}}\gamma_{42} & \frac{\Omega_c}{2} & 0 & \\
0 & 0 & 0 & 0 & 0 & 0 & 0 & 0 & 0 & 0 & 0 & 0 & 0 & \frac{\Omega_c}{2} & -\gamma_{43} & \Delta_{\mathrm{Rf}} \\
0 & 0 & -\frac{\Omega_{\mathrm{Rf}}}{2} & \frac{\Omega_{\mathrm{Rf}}}{2} & 0 & 0 & 0 & 0 & 0 & 0 & 0 & 0 & \frac{\Omega_c}{2} & 0 & \Delta_{\mathrm{Rf}} & \gamma_{43}
\end{pmatrix}. \quad (27)$$

In this way, the problem of solving density matrix in steady state is transformed into a problem of solving linear equations. The key is to solve the inverse of coefficient matrix A. We can use the `linalg.inv` function in `NumPy` module of Python to compute the inverse matrix. The column vector

x can also be obtained directly, using the `numpy.linalg.solve` function. Employing this method to solve the density matrix, the numerical solution of steady-state system can be obtained. At the same time, we also study the method of solving the complex matrix directly. By comparing the efficiency of the two methods, we find the use of our method can double the computational efficiency. In addition, although the method comes from the four-level system; according to this idea, for a N-level system, as long as the problem we want to solve is a steady state, the Hamiltonian of the system can be written as a time-independent matrix under the spin wave approximation, and the diagonal and non-diagonal elements of the density matrix should be defined according to our method. When the master equation is expanded, the diagonal elements correspond to N linearly independent equations, and the non-diagonal elements correspond to $N(N-1)$ linearly independent equations. Note that the sum of the diagonal elements is equal to 1, such as $\sum \rho_{ii} = 1$. As a result, we can get N^2 independent equations, and the density matrix at steady state can be obtained by solving these equations.

4. Effects of Coupling Laser Intensity on the Particle Population

First, calculate the population distribution of different energy levels $|0\rangle$, $|1\rangle$, $|2\rangle$, and $|3\rangle$. Based on the above method, the population distribution of energy levels $|0\rangle$, $|1\rangle$, $|2\rangle$, and $|3\rangle$ depend on $\rho_{11} = x_0$, $\rho_{22} = x_1$, $\rho_{33} = x_2$, and $\rho_{44} = x_4$, respectively. Taking ^{85}Rb atom as an example, let the attenuation rate of the ground state $\Gamma_1 = 0$, the attenuation rate of the D2 line [18, 19] is $\Gamma_2 = 2\pi\times(2$ MHz), and the typical attenuation rate of the Rydberg state are $\Gamma_3 = 2\pi\times(3$ MHz) and $\Gamma_4 = 2\pi\times(2$ MHz). It is assumed that both the probe laser and microwave field resonate with the corresponding energy level, that means $\Delta_p = \Delta_{\mathrm{Rf}} = 0$, the Rabi frequencies of the coupling laser and microwave field are $\Omega_c = \Omega_{\mathrm{Rf}} = 2\pi\times(8$ MHz), respectively. When the Rabi frequency of the probe laser is different, the probe laser is scanned within a certain range, the population distributions of different energy levels can be obtained; see Fig. 2. One can see that the population distributions and the detuning of probe laser at different energy levels are symmetrically distributed. The position of the peaks and troughs of the ground state level $|0\rangle$ is exactly the opposite of that of the Rydberg level $|2\rangle$ and $|3\rangle$. When the probe laser is weak, only a few atoms can be pumped to the Rydberg levels $|2\rangle$ and $|3\rangle$. As the intensity of the probe laser increases, more atoms could be pumped to the Rydberg level $|2\rangle$. For the Rydberg level $|2\rangle$, the structure of the two peaks can be obviously seen. The positions of the two peaks are almost consistent at different Rabi frequencies of the probe laser, the height of the peak increases with increase in the Rabi frequency of the probe laser.

5. Effects of the Laser Intensity on Absorption Characteristics

According to the density matrix theory, it is known that the imaginary part of the off-diagonal element ρ_{21} represents absorption [20], and according to the above theory, it depends on the factor x_5; when the parameters are the same as in the above case, the absorption characteristics can be obtained in the way shown in Fig. 3. From our theoretical calculation, we find the Rabi frequency of the probe laser and the coupling laser only has a little effect on the position of the peak value of the absorption spectrum. The size of the peak is independent of the Rabi frequency of probe laser, but it positively correlates with the Rabi frequency of coupling laser, that means, the larger the Rabi frequency, the smaller the peak value. However, the Rabi frequency of RF laser affects the position of the peak. The greater the Rabi frequency, the greater the distance between the two peaks.

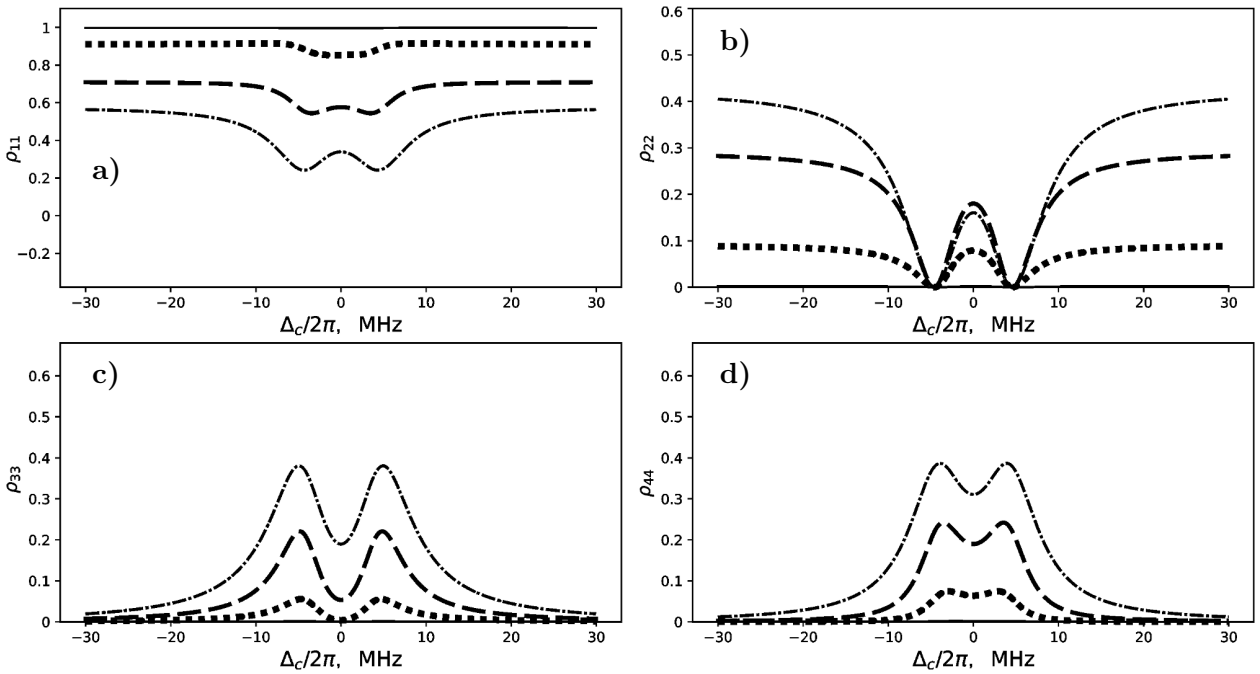

Fig. 2. Variations of the population distributions of different energy levels with the detuning of coupling laser at different Rabi frequencies of state $|0\rangle$ (a), state $|1\rangle$ (b), state $|2\rangle$ (c), and state $|3\rangle$ (d). This data set in numerical calculation is as follows: the Rabi frequencies $\Omega_c = \Omega_{\mathrm{Rf}} = 2\pi\times(8$ MHz), with on-resonant RF and coupling fields ($\Delta_p = \Delta_{\mathrm{Rf}} = 0$). Here, $\Omega_p = 2\pi \cdot 0.3$ MHz (the solid curve), $\Omega_p = 2\pi \cdot 2$ MHz (the dotted curve), $\Omega_p = 2\pi \cdot 5$ MHz (the dashed curve), and $\Omega_p = 2\pi \cdot 10$ MHz (the dash-dotted curve).

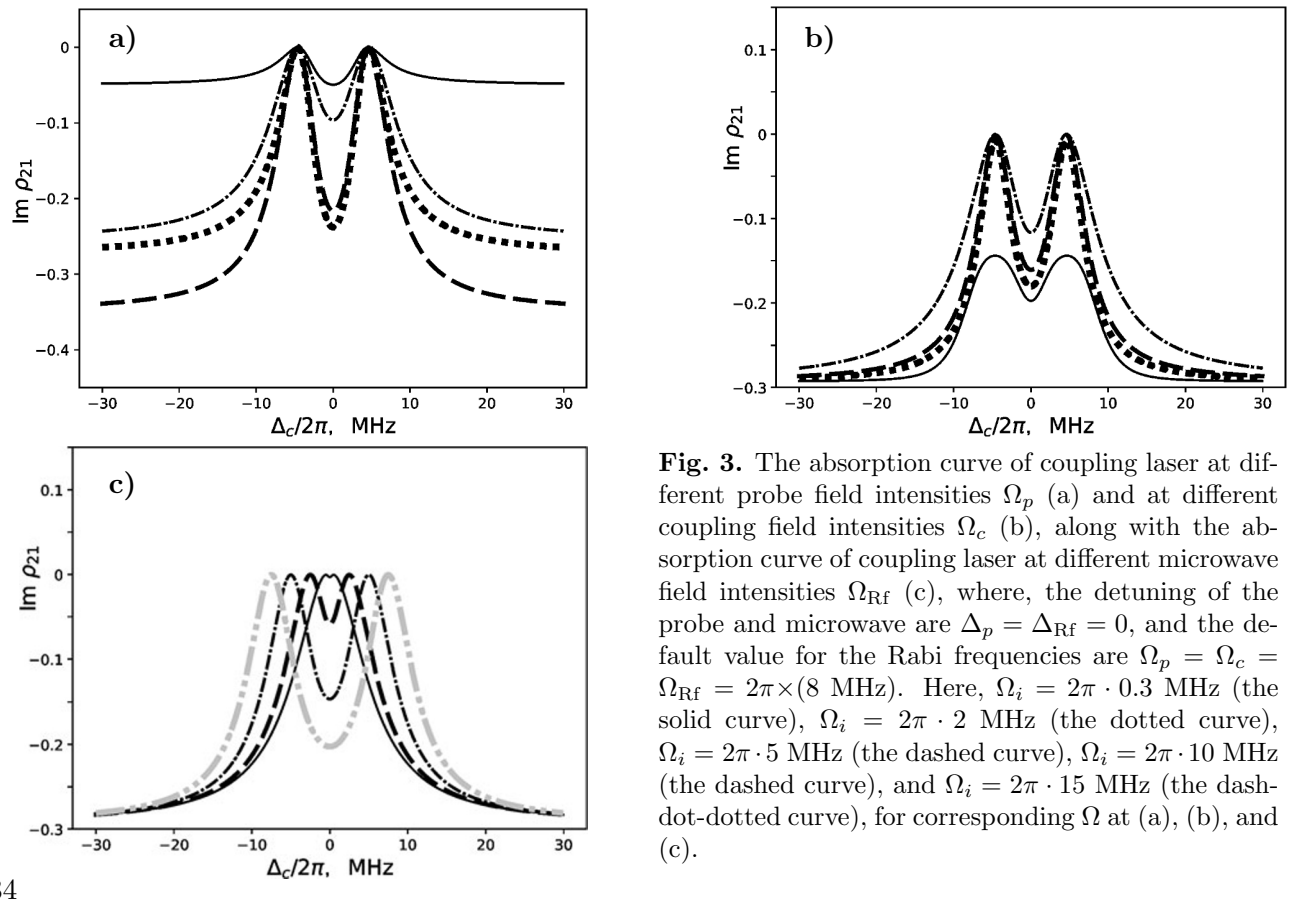

Fig. 3. The absorption curve of coupling laser at different probe field intensities Ω_p (a) and at different coupling field intensities Ω_c (b), along with the absorption curve of coupling laser at different microwave field intensities Ω_{Rf} (c), where, the detuning of the probe and microwave are $\Delta_p = \Delta_{\mathrm{Rf}} = 0$, and the default value for the Rabi frequencies are $\Omega_p = \Omega_c = \Omega_{\mathrm{Rf}} = 2\pi\times(8$ MHz). Here, $\Omega_i = 2\pi \cdot 0.3$ MHz (the solid curve), $\Omega_i = 2\pi \cdot 2$ MHz (the dotted curve), $\Omega_i = 2\pi \cdot 5$ MHz (the dashed curve), $\Omega_i = 2\pi \cdot 10$ MHz (the dashed curve), and $\Omega_i = 2\pi \cdot 15$ MHz (the dash-dot-dotted curve), for corresponding Ω at (a), (b), and (c).

6. Nonlinearity of EIT Signal

With the microwave electric field coupling to the Rydberg energy level, the EIT signal would be split. The observed splitting of the two peaks is referred to as AT splitting, which is usually expressed as Δ_f, which is related to the Rabi frequency. The Rabi frequency is proportional to the intensity of the microwave field $|E_{\mathrm{Rf}}|$; it reads

$$2\pi\Delta f = \Omega_{\mathrm{Rf}} = \frac{\mathcal{P}}{\hbar}|E_{\mathrm{Rf}}|. \tag{28}$$

However, it was experimentally found that the two are not absolutely proportional, there is a nonlinear relationship within a certain range [6]. In order to explain this phenomenon, based on the above theory and on the premise of obtaining the imaginary part of the off-diagonal element of the density matrix ρ_{21}, the influence of the atomic velocity distribution needs to be considered. We add the atomic velocity distribution with the convolution method [18, 21],

$$\rho_{21D} = \frac{1}{u\sqrt{\pi}} \int \rho_{21}(\Delta_p', \Delta_c')\, e^{-v^2/u^2}\, dv, \tag{29}$$

where the shifted detunings are $\Delta_p' = \Delta_p - \dfrac{2\pi}{\lambda_p} v$ and $\Delta_c' = \Delta_c - \dfrac{2\pi}{\lambda_c} v$, the factors λ_p and λ_c represent the wavelength of the probe laser and the coupling laser, respectively. In the calculations, the values are set as $\lambda_p = 780$ nm and $\lambda_c = 480$ nm [21]. Also, $u = \sqrt{2k_B T/m}$ is the most probable speed of Rydberg atomic gas, k_B is Boltzmann constant, m is the atom mass of ^{85}Rb, and T represents the absolute temperature. As a result, we see that the value of ρ_{21D} is affected by temperature. In Fig. 4, we show the relationship between the Rabi frequency of microwave field and AT splitting, from which we can see that the Rabi frequency of microwave electric field affects the position of EIT double peaks. For our Rb atomic system, when $\Omega_{\mathrm{Rf}}/2\pi > 0.3$ MHz, the distance between the double peaks and the Rabi frequency of microwave electric field basically shows a linear relationship, this range is an effective

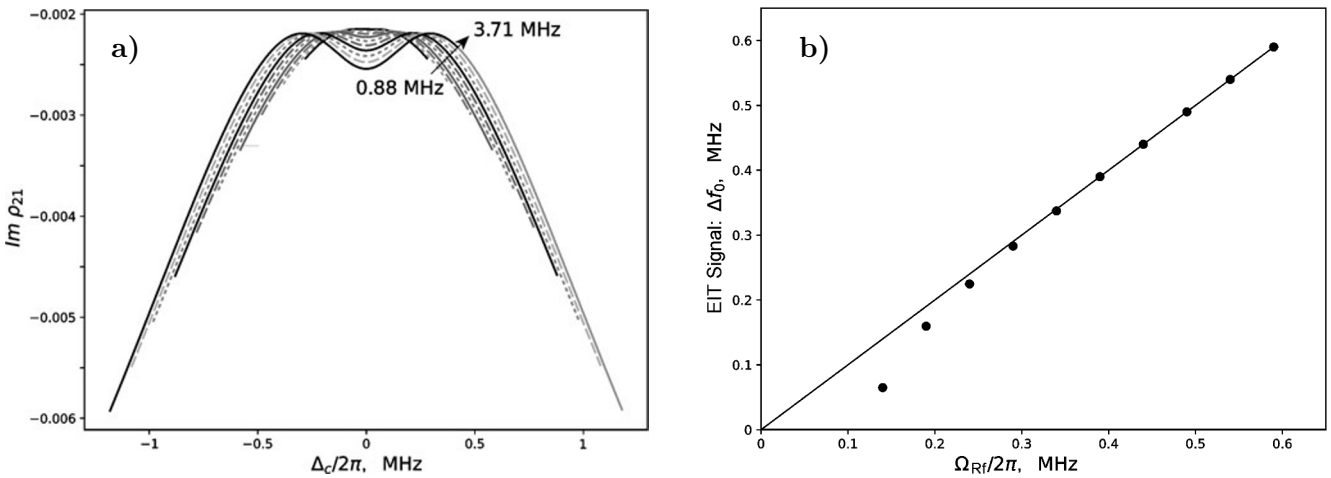

Fig. 4. Absorption characteristic curve of microwave field with different Rabi frequencies $\Omega_{\mathrm{Rf}} = 2\pi \cdot (0.88, 1.19, 1.51, 1.82, 2.14, 2.45, 2.76, 3.08, 3.39, 3.71)$ MHz from bottom to top (a) and the relationship between bimodal distance of EIT signal and Rabi frequency of microwave field (b). The default data set is the same as described in Fig. 3.

area for accurate measuring the intensity of microwave electric field, using the Rydberg atomic gas. In contrast, when $\Omega_{\rm Rf}/2\pi < 0.3$ MHz, there is a nonlinear relationship between the EIT bimodal distance and the Rabi frequency of microwave electric field, this area should be avoided as far as possible in the experiment.

In addition, we study the relationship between the splitting width of EIT signal Δ_f and the microwave field Rabi frequency $\Omega_{\rm Rf}$ at different decay rates Γ_2. We find that the range of the linear region is related to Γ_2; in Fig. 5, we can see that the greater decay rate Γ_2, the wider the linear range.

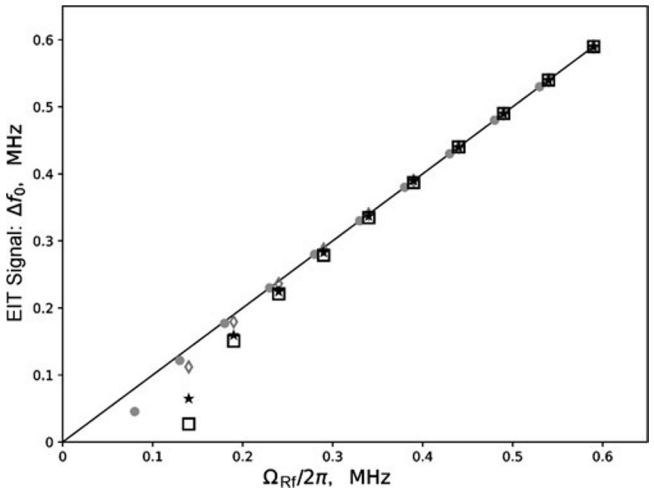

Fig. 5. The relationship between Δ_f and $\Omega_{\rm Rf}$ at different decay rates Γ_2. Here, $\Gamma_2 = 2\pi\times(20$ MHz) (●), $\Gamma_2 = 2\pi\times(9.79$ MHz) (◊), $\Gamma_2 = 2\pi\times(6.06$ MHz) (⋆), and $\Gamma_2 = 2\pi\times(5.23$ MHz) (□) are the typical decay rates of Sodium (Na), Rubidium (Rb), and Cesium (Cs), respectively.

7. Summary

Based on the density matrix theory, in this paper, we studied the steady-state solution of a four-level Rydberg atomic system under multiple laser fields. In order to solve the evolution equation of density matrix, we constructed a matrix, in which the diagonal elements were real and the off-diagonal elements were complex, which makes sense in physics. Also, we studied the advantage of this construction method and found that it could double the computation speed. Based on this method, we quantitatively discussed the influence of the intensity of the probe laser on the population distribution when coupling laser and microwave field were in resonance. In addition, we investigated the influence of the intensity of the probe laser on the absorption characteristics of energy levels. We used the convolution method to introduce the Doppler effect and, on this basis, we studied the nonlinear relationship between the intensity of microwave field and the absorption characteristics.

Acknowledgments

The authors would like to acknowledge the financial support from Science and Technology Department of Henan Province under Grant No. 212102210464.

References

1. J. A. C. Gallas, G. Leuchs, H. Walther, and H. Figger, *Adv. At. Mol. Phys.*, **20**, 413 (1985).
2. E. Brion, K. Mølmer, and M. Saffman, *Phys. Rev. Lett.*, **99**, 260501 (2007).
3. M. Saffman and K. Mølmer, *Phys. Rev. A*, **78**, 012336 (2008).
4. L. Isenhower, E. Urban, X. L. Zhang, et al., *Phys. Rev. Lett.*, **104**, 010503 (2010).
5. J. A. Sedlacek, A. Schwettmann, H. Kübler, et al., *Nat. Phys.*, **8**, 819 (2012).
6. C. Fabre and S. Haroche, *Opt. Commun.*, **15**, 254 (1975).
7. D. V. Ponomarenko and A. F. Shestakov, *Chem. Phys. Lett.*, **210**, 269 (1993).
8. J. Zhao, H. Zhang, Z. Feng, et al., *J. Phys. Soc. Jpn.*, **80**, 034303 (2011).

9. M. O. Scully and M. S. Zubairy, *Quantum Optics*, Cambridge University Press (1997).
10. A. Imamoğlu and S. E. Harris, *Opt. Lett.*, **14**, 1344 (1989).
11. K.-J. Boller, A. Imamoğlu, and S. E. Harris, *Phys. Rev. Lett.*, **66**, 2593 (1991).
12. J. A. Sedlacek, A. Schwettmann, H. Kübler, et al., *Nat. Phys.*, **8**, 819 (2012).
13. D. A. Anderson, S. A. Miller, G. Raithel, et al., *Phys. Rev. Appl.*, **5**, 034003 (2016).
14. A. K. Mohapatra, T. R. Jackson, and C. S. Adams, *Phys. Rev. Lett.*, **98**, 113003 (2007).
15. A. K. Mohapatra, M. G. Bason, B. Butscher, et al., *Nat. Phys.*, **4**, 890 (2008).
16. S. Mauger, J. Millen, and M. P. A. Jones, *J. Phys. B: At. Mol. Opt. Phys.*, **40**, F319 (2007).
17. L. Hao, Y. Xue, J. Fan, et al., *Appl. Sci.*, **9**, 1720 (2019).
18. C. L. Holloway, M. T. Simons, J. A. Gordon, et al., *J. Appl. Phys.*, **121**, 233106 (2017).
19. D. A. Steck, `steck.us/alkalidata/rubidium85numbers.pdf` (revision 2.3.2, September 10, 2023).
20. P. R. Berman and V. S. Malinovsky, *Principles of Laser Spectroscopy and Quantum Optics*, Princeton Univerity Press (2011).
21. F. Zhou, F. D. Jia, J. Mei, et al., *J. Phys. B: At. Mol. Opt. Phys.*, **55**, 075501 (2022).